POLITECNICO DI TORINO
Repository ISTITUZIONALE

Broadband vibration energy harvesting using nonlinear multi degree-of-freedom mechanical filters

Original
Broadband vibration energy harvesting using nonlinear multi degree-of-freedom mechanical filters / Song, K., Bonnin, M., Traversa, F.L., Bonani, F.. - In: NONLINEAR DYNAMICS. - ISSN 0924-090X. - ELETTRONICO. - 113:12(2025), pp. 14301-14317. [10.1007/s11071-025-10950-6]

Availability:
This version is available at: 11583/2999055 since: 2025-04-11T02:59:18Z

Publisher:
Springer Nature

Published
DOI:10.1007/s11071-025-10950-6

Terms of use:

This article is made available under terms and conditions as specified in the corresponding bibliographic description in the repository

Publisher copyright

(Article begins on next page)

10 September 2026

Nonlinear Dyn
https://doi.org/10.1007/s11071-025-10950-6

RESEARCH

Broadband vibration energy harvesting using nonlinear multi degree-of-freedom mechanical filters

Kailing Song · Michele Bonnin · Fabio L. Traversa · Fabrizio Bonani

Received: 27 October 2024 / Accepted: 28 January 2025
© The Author(s) 2025

Abstract We introduce the model of a networked energy harvester for random ambient vibrations, made of mechanically coupled oscillators. The networked harvester is equivalent to a mechanical filter, and it can be modeled as a chain of masses, coupled pairwise by nonlinear elastic springs. Ambient mechanical vibrations are modeled as a low-pass filtered white Gaussian noise, and a piezoelectric transducer is used to convert mechanical kinetic energy into electrical energy. We derive the nonlinear equations of motion for the harvester, together with formulas for the average harvested power and power efficiency. An approximate analytical solution is presented and compared with numerical simulations. Finally, we discuss the optimization of the networked harvester, based on a gradient ascent algorithm combined with Nesterov's momentum method. We show that, after proper optimization, the mechanically coupled energy harvester scavenges more power than a single mass-spring energy harvester.

K. Song · M. Bonnin (✉) · F. Bonani
Department of Electronics and Telecommunications, Politecnico di Torino, Turin, Italy
e-mail: michele.bonnin@polito.it

F. Bonani
e-mail: fabrizio.bonani@polito.it

K. Song
University School for Advanced Studies, IUSS, Pavia, Italy
e-mail: kailing.song@polito.it

F. L. Traversa
MemComputing Inc., San Diego, CA, USA
e-mail: ftraversa@memcpu.com

Keywords Energy harvesting · Mechanical vibrations · Electro-mechanical systems · Nonlinear dynamics · Stochastic processes · Stochastic differential equations · Machine learning · Gradient descent/ascent

1 Introduction

As the demand for energy continues to escalate alongside the global push for reduced carbon footprints, innovative methods of energy capture are critical. In the recent years, energy harvesting has emerged as a pivotal technology in the pursuit of sustainable energy solutions, enabling the conversion of energy dispersed in the environment that would otherwise be wasted, into usable electrical power [1–3].

By integrating energy harvesting technologies into everyday applications, such as wearable devices, remote sensors, and smart infrastructure, we can develop autonomous, self-sustaining systems that can operate indefinitely in various conditions, decreasing the need for disposable batteries and contributing to reduce electronic waste [4–7]. This aligns with global sustainability goals and reduces the ecological footprint of deployed sensor networks. Energy harvesting can also contribute to more reliable operation by providing a continuous power source. This minimizes the risk of unexpected device failures due to battery exhaustion, ensuring that critical systems remain operational. By harnessing ambient energy, devices can maintain func-

Published online: 12 February 2025

tionality for extended periods without battery depletion. This is particularly beneficial for applications in hard-to-reach locations where battery replacement is challenging, such as in infrastructure monitoring or environmental sensing. Moreover, reducing battery use, maintenance efforts and costs are decreased, as frequent battery replacement can be costly and inconvenient.

Candidate energy sources for supplying power to wireless sensors and actuators networks include mechanical vibrations [8–12], electromagnetic waves [13,14], and thermal gradients [15–17]. Mechanical vibrations are particularly important, because they are ubiquitous, versatile, and they are characterized by relatively high power density. Specifically, mechanical vibrations may have natural origin, like wind, seismic activity, or even animal and human motion, or may result from man-made activities, like transportation systems (road vehicles, trains and airplanes), household and industrial machinery, or structural responses in bridges and buildings. They are versatile because different transduction mechanisms can be exploited for their conversion into electrical power, including piezoelectricity [18–23], electromagnetic induction [12,24–30], and magnetostrictive phenomena [31–34].

In essence, energy harvesters are mechanical resonators. If the frequency of external vibrations is close to their resonant frequency, they will exhibit large amplitude oscillations, collecting a significant amount of energy. However, linear resonators are inherently characterized by narrow bandwidth, meaning that vibrations with frequencies far from resonance give little contribution to the harvested energy. This is an important limiting factor, because in most practical applications mechanical vibrations result from the superposition of several spectral components, and their power is distributed over a wide frequency interval. To overcome the issue, different ingenious solutions have been proposed in the past few years [35–40].

Recently, we have shown that the interposition of a reactive matching network between the transducer and the electrical load, increases the harvested power and the power efficiency by a significant amount, even for nonlinear, multi-stable systems [41–44]. The main drawback of the proposed solution is that a relatively large inductance is required in the matching network, to compensate for the negative reactance of the mechanical resonator, a well known limitation in matching mechanical-to-electrical systems [45].

In this work, we propose a novel solution to achieve similar results while avoiding the limitations mentioned above. We consider a networked energy harvester, composed of mechanically coupled resonators. The networked harvester can be schematically modeled as a chain of masses, coupled pairwise by nonlinear elastic springs, equivalent to a mechanical filter. Like their electrical counterparts, mechanical filters are designed to pass a range of signal frequencies, while blocking others. The challenge is to design a filter with a wide pass-band in the spectral region where most of vibrational energy is concentrated, without sacrificing too much oscillation amplitude at the central frequency. The matching is entirely done in the mechanical domain, by a proper choice of the masses and the spring elastic constants (both linear and nonlinear), therefore avoiding the need of large inductances.

In the last few years several works considered coupled energy harvesters [46–53]. Both mechanical and magnetic couplings have been proposed and experimentally analyzed. In [46], the coupling is obtained connecting the harvesters by a rod and exploiting both rotational and translational displacements. In [47], a two DOF structure is obtained considering two cantilever-mass structures, a primary cantilever of length l_1 and a secondary beam of length l_2 cut inside the primary. In [48] a magnetic coupling between two cantilevers is introduced by tip magnets. The authors show that the magnetic interaction is equivalent to a coupling through a spring. A similar arrangement is considered in [49]. Other examples of magnetically coupled harvesters can be found in [50–52]. The design of these multi DOF structures can be viewed as a mechanical impedance matching problem.

We derive semi-analytical formulas for the average harvested power and the power efficiency, that are used to optimize the networked harvester's parameters. We apply a gradient ascent method, combined with Nesterov's momentum, for the system optimization. The proposed optimization method is very efficient and convergences very rapidly. We show that the networked energy harvester offers significantly more power than the simple single mass-spring system. Theoretical results are validated through numerical simulations.

The paper is organized as follows: In Sect. 2 we introduce the model for the networked energy harvester based on coupled resonators. In Sect. 3 we present some analytical results, and we discuss approximate

expressions for the average output power and the power efficiency. Section 4 is devoted to introducing the systematic procedure for the optimization of the energy harvester. The algorithm for the maximization of the desired output function is presented, based on the gradient ascent method combined with Nesterov's momentum. Numerical results referring to a practical application are discussed in Sect. 5. Finally, Sect. 6 is devoted to conclusions.

2 Multi degree-of-freedom energy harvester modeling

The schematic representation of a single mechanical degree-of-freedom (DOF) energy harvester for ambient mechanical vibrations is shown in Fig. 1a. The harvester is composed of an oscillating structure, represented by a mass m and a spring with elastic potential $U(q)$, where q is the displacement from the resting position, that captures kinetic energy from ambient vibrations. Internal friction is accounted for by a damping coefficient denoted as γ. Mechanical vibrations act as an external force $f_{\text{ext}}(t)$, that excites oscillations of the mass-spring structure. The oscillating system is connected to a transducer, which is responsible for converting the mechanical kinetic energy into usable electrical power, that in turn is made available to the electrical load through the output voltage $v(t)$. Different conversion mechanisms can be exploited, including piezoelectric, magneto-restrictive, electrostatic, and electromagnetic [54,55]. Therefore, the transducer provides a coupling between the mechanical and the electrical domains of the harvester irrespective of the conversion physical principle. Through the transducer, kinetic energy is converted into a voltage proportional to the displacement, while in turn, the electrical part exerts a force on the mechanical domain, that is proportional to the output voltage. The coupling is usually so small that the relationships can be assumed linear [41].

In this work, we consider an extension of the energy harvester described above, to the case of a multiple mechanical DOF, as schematically represented in Fig. 1b. The harvester is composed of n masses m_j, coupled pairwise through springs with elastic potentials $U_j(q_j, q_{j+1}) \geq 0$ (for $j = 1, \ldots, n$), where q_j is the displacement of the j-th mass. Notice that, since the n-th spring is connected to the transducer, we have $q_{n+1} = 0$.

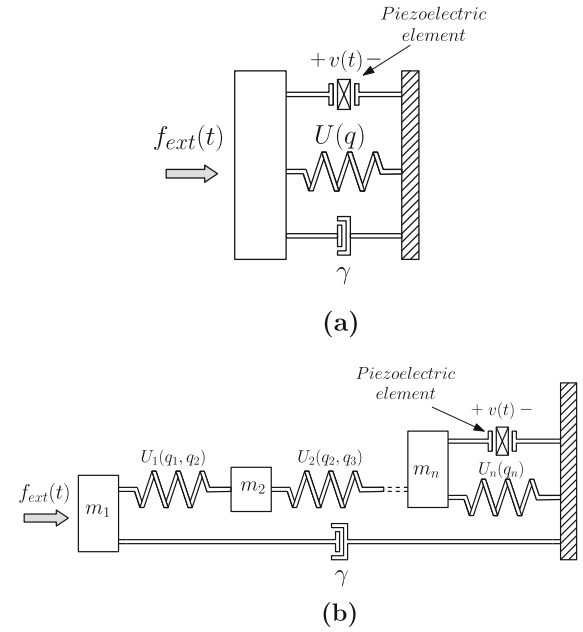

Fig. 1 Schematic representation of an energy harvester for ambient mechanical vibrations. The piezoelectric element represents the transducer. **a** Single DOF. **b** Multi DOF

Such a structure is a mechanical filter, that acts on mechanical vibrations (including sound waves) in the very same way an electrical filter acts on electrical signals. Electrical filters are designed to pass a range of signal frequencies, while blocking others. Similarly, mechanical filters are usually intended to reduce vibrations and noise. Just like passive electrical filters are composed by reactive elements (capacitors and inductors), mechanical filters are composed by resonators which, irrespective of the constructive technique, can be represented by coupled masses and springs. Our goal is to design the filter that passes as many frequencies as possible, transferring the maximum available power to the electrical load.

Collecting the displacements into a single vector $\mathbf{q} = [q_1, \ldots, q_n]^T$, the Lagrangian function for the n-tuple mass-spring pairs is

$$\mathcal{L}(\mathbf{q}, \dot{\mathbf{q}}) = \sum_{j=1}^{n} \frac{1}{2} m_j \dot{q}_j^2 - \sum_{j=1}^{n} U_j(q_j, q_{j+1}) \tag{1}$$

Concerning the dissipative part of the system, to keep the model reasonably simple, we shall assume that the friction effects are negligible, except for the first

mass. Although such an assumption cannot be rigorously justified *a priori*, our numerical simulations show that the displacement for the first mass is significantly larger than all others, thus justifying to some extent the assumption. For small values of the damping coefficient γ, the dissipation potential takes the form $\mathcal{D}(q_1) = \gamma\, \dot{q}_1^2/2$. Therefore the Lagrange equations of motion for the mechanical part read

$$m_j \ddot{q}_j + \gamma \dot{q}_j \delta_{1j} + \frac{\partial U_j(q_j, q_{j+1})}{\partial q_j} + \frac{\partial U_{j-1}(q_{j-1}, q_j)}{\partial q_j} = F_j(t), \qquad j = 1, \ldots, n \tag{2}$$

where $q_0 = q_{n+1} = 0$, $U_0 = 0$, δ_{ij} is the Kronecker delta, and $F_j(t)$ is the resultant of the forces applied to the j-th mass, in particular

$$F_j(t) = \begin{cases} f_{\text{ext}}(t) & \text{for} \quad j = 1 \\ 0 & \text{for} \quad j = 2, \ldots, n-1 \\ -\alpha\, v & \text{for} \quad j = n \end{cases} \tag{3}$$

with α being the electro-mechanical coupling constant (in N/V or As/m). Thus (2) can be rewritten in the more compact form

$$m_j \ddot{q}_j + \frac{\partial U_j(q_j, q_{j+1})}{\partial q_j} + \frac{\partial U_{j-1}(q_{j-1}, q_j)}{\partial q_j} + (\gamma \dot{q}_j - f_{\text{ext}}(t))\delta_{1j} + \alpha\, v\, \delta_{nj} = 0, \quad j = 1, \ldots, n \tag{4}$$

Assuming that the electrical load is a simple resistor with resistance R (and conductance $G = 1/R$), the output voltage satisfies the differential equation [42–44]

$$\dot{v} = \frac{\alpha}{C_{\text{pz}}} \dot{q}_n - \frac{G}{C_{\text{pz}}} v \tag{5}$$

where C_{pz} is the electrical capacitance of the piezoelectric transducer.

Finally, we consider the external force modeling mechanical vibrations. Since in nature most ambient vibrations are inherently random, we model the force $f_{\text{ext}}(t)$, as a stochastic process Z_t. For notation, we shall use upper-case letters to denote stochastic processes, and lower-case letters for their values.

The typical frequency of ambient vibrations ranges from a few Hz for human motion, to some hundreds of Hz for domestic and industrial machinery [56]. Consequently, a proper stochastic process modeling ambient vibrations is a band limited white Gaussian noise, also known as the Ornstein–Uhlenbeck process [57,58]. The Ornstein–Uhlenbeck process is the solution of the stochastic differential equation (SDE)

$$dZ_t = -\frac{1}{\tau} Z_t dt + \frac{D}{\tau} dW_t \tag{6}$$

where W_t is a Wiener process (the integral of a white Gaussian noise), characterized by expectation $\mathrm{E}[W_t] = 0$, covariance $\mathrm{cov}(W_t, W_s) = \mathrm{E}[W_t W_s] = \min(t, s)$ and $W_t \sim \mathcal{N}(0, t)$, where symbol $\sim$ means "distributed as", and $\mathcal{N}(0, t)$ is the normal distribution, centered at zero. The Ornstein–Uhlenbeck process with deterministic initial condition Z_0 is characterized by the expectation

$$\mathrm{E}[Z_t] = Z_0 \exp\left(-\frac{t}{\tau}\right) \tag{7}$$

by the covariance

$$\mathrm{cov}(Z_t, Z_s) = \frac{D^2}{2\tau}\left[\exp\left(\frac{|t-s|}{\tau}\right) - \exp\left(\frac{t+s}{\tau}\right)\right] \tag{8}$$

and by the power spectral density (PSD):

$$S_{\text{OU}}(\omega) = \frac{D^2}{1 + \omega^2 \tau^2} \tag{9}$$

Combining together (4)–(6), introducing the conjugate momenta $p_j = m_j \dot{q}_j$, and rewriting as a system of first order SDEs, we obtain:

$$dQ_j = \frac{1}{m_j} P_j\, dt \tag{10a}$$

$$dP_j = \left[-\frac{\partial U_j(Q_j, Q_{j+1})}{\partial Q_j} - \frac{\partial U_{j-1}(Q_{j-1}, Q_j)}{\partial Q_j} + \left(Z_t - \frac{\gamma}{m_j} P_j\right)\delta_{1j} - \alpha V \delta_{nj}\right] dt \quad j = 1, \ldots, n \tag{10b}$$

$$dV = \left(\frac{\alpha}{C_{\text{pz}}} \frac{P_n}{m_n} - \frac{G}{C_{\text{pz}}} V\right) dt \tag{10c}$$

$$dZ_t = -\frac{1}{\tau} Z_t\, dt + \frac{D}{\tau} dW_t \tag{10d}$$

Because noise in Eq. (10) is un-modulated (or additive), the solution of the SDE system does not depend on the interpretation adopted: In what follows we shall interpret all SDEs as Itô equations.

3 Theoretical analysis

We are interested in the average power scavenged by the energy harvester, and in the associated power conversion efficiency. To calculate these quantities, we consider the total energy stored in the harvester, which is the sum of the kinetic energies of the masses, of the elastic potential energies of the springs, and of the electrical energy stored in the transducer:

$$E = \sum_{j=1}^{n} \left(\frac{P_j^2}{2m_j} + U_j(Q_j, Q_{j+1}) \right) + \frac{1}{2} C_{\mathrm{pz}} V^2 \quad (11)$$

Application of Itô formula [57,59] to Eq. (11), combined with (10), yields (see appendix):

$$dE = \left(P_1 Z_t / m_1 - \gamma P_1^2 / m_1^2 - G V^2 \right) dt \quad (12)$$

Taking expectations, we obtain the power balance equation:

$$\mathrm{E}\left[\frac{dE}{dt}\right] = \frac{1}{m_1}\mathrm{E}[P_1 Z_t] - \frac{\gamma}{m_1^2}\mathrm{E}\left[P_1^2\right] - G\,\mathrm{E}\left[V^2\right] \quad (13)$$

Adopting the passive sign convection, the first term on the right hand side represents the average power injected by noise into the harvester: $P_{\mathrm{in}} = \mathrm{E}[P_1 Z_t]/m_1$. The second term, represents the power dissipated by internal friction: $P_{\mathrm{dis}} = \gamma \mathrm{E}\left[P_1^2\right]/m_1^2$. Finally, the last term is the average harvested power: $P_{\mathrm{out}} = G\,\mathrm{E}[V^2]$. Consequently, the power efficiency of the harvester is:

$$\eta = \frac{P_{\mathrm{out}}}{P_{\mathrm{in}}} = m_1 G \frac{\mathrm{E}\left[V^2\right]}{\mathrm{E}[Z_t P_1]} \quad (14)$$

These equations show that to evaluate the harvested power and the power efficiency, we need to calculate the second moments of the distribution of the stochastic process $\mathbf{X}_t = [Q_1, P_1, \ldots, Q_n, P_n, V, Z]^T$.

Let us denote the state vector of size $2n+2$

$$\mathbf{x} = [q_1, p_1, \ldots, q_n, p_n, v, z]^T$$

and let $\mathcal{B}(\overline{\mathbf{x}})$ be a neighborhood of the point

$$\overline{\mathbf{x}} = [\overline{q}_1, 0, \ldots, \overline{q}_n, 0, 0, 0]^T$$

As a preliminary result, we study the equilibrium points of system (10) in the absence of noise, i.e. when the SDE system reduces to a deterministic, homogeneous ordinary differential equation (ODE) system.

Theorem 1 *If the potentials $U_j(q_j, q_{j+1})$ have a local minimum at $(\overline{q}_j, \overline{q}_{j+1})$ for all $j = 1, \ldots, n$, then system (10) for $D = 0$ has an asymptotically stable equilibrium point at $\mathbf{x} = \overline{\mathbf{x}}$.*

Proof Without loss of generality, we assume that the local minimum is $U_j(\overline{q}_j, \overline{q}_{j+1}) = 0$. Thus, $U_j(q_j, q_{j+1}) \geq 0$ for all q_j, q_{j+1} in a neighborhood of the minimum. It is straightforward seeing that, if $D = 0$, $\mathbf{x} = \overline{\mathbf{x}}$ is an equilibrium point of (10). To prove that the equilibrium point is asymptotically stable, consider the function $\mathcal{V} : \mathbb{R}^{2n+2} \mapsto \mathbb{R}$:

$$\mathcal{V}(\mathbf{x}) = \sum_{j=1}^{n} \left(\frac{p_j^2}{2m_j} + U_j(q_j, q_{j+1}) \right) + \frac{1}{2} C_{\mathrm{pz}} v^2 + \beta z^2$$

where $\beta > 0$ is a real constant. By definition, $\mathcal{V}(\mathbf{x}) > 0$ for all $\mathbf{x} \in \mathcal{B}(\overline{\mathbf{x}})$, $\mathbf{x} \neq \overline{\mathbf{x}}$, and $\mathcal{V}(\overline{\mathbf{x}}) = 0$. Using (10) (with $D = 0$), we find

$$\dot{\mathcal{V}}(\mathbf{x}) = -\frac{\gamma}{m_1^2} p_1^2 + \frac{z\, p_1}{m_1} - G\, v^2 - \frac{2\beta}{\tau} z^2 \quad (15)$$

Choosing $\beta = \tau/(8\gamma)$ we obtain

$$\dot{\mathcal{V}}(\mathbf{x}) = -\gamma \left(\frac{p_1}{m_1} - \frac{z}{2\gamma} \right)^2 - G\, v^2 \quad (16)$$

Then $\dot{\mathcal{V}}(\mathbf{x}) < 0$ for all $\mathbf{x} \in \mathcal{B}(\overline{\mathbf{x}})$ and $\mathbf{x} \neq \overline{\mathbf{x}}$, which implies that $\mathcal{V}$ is a strict Lyapunov function [60], and therefore $\overline{\mathbf{x}}$ is asymptotically stable. □

3.1 Linear system analysis

First, we consider the case of a linear mechanical system, that corresponds to elastic potentials such that

$U_j = \mathcal{O}(||\mathbf{x}||^2)$. Without loss of generality, we assume that the equilibrium point is at $\bar{\mathbf{x}} = 0$. The SDE system (10) can be rewritten in the compact form:

$$d\mathbf{X}_t = \mathbf{A}\,\mathbf{X}_t\,dt + \mathbf{B}\,dW_t \tag{17}$$

where $\mathbf{X}_t = [Q_1, P_1, \ldots, Q_n, P_n, V, Z]^T \in \mathbb{R}^{2n+2}$ is the state vector, $\mathbf{B} = [0, \ldots, 0, D/\tau]^T \in \mathbb{R}^{2n+2}$ is the diffusion vector, and $\mathbf{A} \in \mathbb{R}^{(2n+2)\times(2n+2)}$ is the matrix of the drift coefficients. Thanks to Theorem 1 and to the fact that, for a linear homogeneous system, asymptotic stability implies hyperbolicity, matrix $\mathbf{A}$ is stable.

The SDE system (17) is a multivariate Ornstein–Uhlenbeck process [57,59], and consequently $\mathbf{X}_t$ is characterized by a multivariate normal distribution. The expectations are easily calculated. Taking the expectation of (17) and using the fact that $\mathbf{A}$ is stable, it follows that, asymptotically for $t \to +\infty$, $\mathrm{E}[\mathbf{X}_t] = 0$. For the second order moments, using (17) and Itô formula we obtain:

$$\begin{aligned} d(\mathbf{X}_t\mathbf{X}_t^T) = &\left(\mathbf{A}\,\mathbf{X}_t\mathbf{X}_t^T + \mathbf{X}_t\mathbf{X}_t^T\mathbf{A}^T + \mathbf{B}\mathbf{B}^T\right)dt \\ &+ \left(\mathbf{B}\mathbf{X}_t^T + \mathbf{X}_t\mathbf{B}^T\right)dW_t \end{aligned} \tag{18}$$

Taking again the expectation yields

$$\frac{d\boldsymbol{\Sigma}}{dt} = \mathbf{A}\boldsymbol{\Sigma} + \boldsymbol{\Sigma}\mathbf{A}^T + \mathbf{B}\mathbf{B}^T \tag{19}$$

where $\boldsymbol{\Sigma} = \mathrm{E}[\mathbf{X}_t\mathbf{X}_t^T]$ is the covariance matrix.

Matrix equation (19) can be recast in vector form using vectorization. Let $\boldsymbol{\Sigma}_i \in \mathbb{R}^{2n+2}$, $i = 1, \ldots, 2n+2$, be the columns of $\boldsymbol{\Sigma}$, the vectorization operation is defined by stacking the columns of $\boldsymbol{\Sigma}$ into the vector $\boldsymbol{\sigma} \in \mathbb{R}^{(2n+2)(2n+2)}$:

$$\boldsymbol{\sigma} = \mathrm{vec}(\boldsymbol{\Sigma}) = \begin{bmatrix} \boldsymbol{\Sigma}_1 \\ \vdots \\ \boldsymbol{\Sigma}_{2n+2} \end{bmatrix} \tag{20}$$

Using the property

$$\mathrm{vec}(\mathbf{A}\boldsymbol{\Sigma} + \boldsymbol{\Sigma}\mathbf{A}^T) = (\mathbf{I}\otimes\mathbf{A} + \mathbf{A}\otimes\mathbf{I})\,\mathrm{vec}(\boldsymbol{\Sigma}) \tag{21}$$

where $\mathbf{I}$ is the identity matrix of size $2n+2$, and $\otimes$ is the Kronecker product, Eq. (19) becomes the linear ODE system

$$\frac{d\boldsymbol{\sigma}}{dt} = (\mathbf{I}\otimes\mathbf{A} + \mathbf{A}\otimes\mathbf{I})\boldsymbol{\sigma} + \mathbf{w} \tag{22}$$

where $\mathbf{w} = \mathrm{vec}(\mathbf{B}\mathbf{B}^T)$.

We shall now prove that linear system (22) is well posed, i.e. its solution is unique and the components of $\boldsymbol{\sigma}$ are bounded for all $t \geq 0$.

Theorem 2 *Let λ_i be the eigenvalues of $\mathbf{A}$, and let $\mathbf{v}_i$ be the corresponding eigenvectors. Then matrix $(\mathbf{I}\otimes\mathbf{A} + \mathbf{A}\otimes\mathbf{I})$ has eigenvalues $2\lambda_i$ with eigenvectors $(\mathbf{v}_i\otimes\mathbf{v}_i)$.*

Proof To prove the result we use the following two properties of the Kronecker product:

1. Multiplication by a scalar: Let $\alpha \in \mathbb{R}$, $\mathbf{A} \in \mathbb{R}^{n_1\times n_2}$ and $\mathbf{B} \in \mathbb{R}^{n_3\times n_4}$, then

   $$(\alpha\mathbf{A})\otimes\mathbf{B} = \mathbf{A}\otimes(\alpha\mathbf{B}) = \alpha(\mathbf{A}\otimes\mathbf{B})$$

2. The product of two Kronecker products yields another Kronecker product: Let $\mathbf{A} \in \mathbb{R}^{n_1\times n_2}$, $\mathbf{B} \in \mathbb{R}^{n_3\times n_4}$, $\mathbf{C} \in \mathbb{R}^{n_2\times n_5}$ and $\mathbf{D} \in \mathbb{R}^{n_4\times n_6}$, then:

   $$(\mathbf{A}\otimes\mathbf{B})(\mathbf{C}\otimes\mathbf{D}) = (\mathbf{A}\mathbf{C})\otimes(\mathbf{B}\mathbf{D})$$

Applying these two properties we have:

$$\begin{aligned} &(\mathbf{I}\otimes\mathbf{A} + \mathbf{A}\otimes\mathbf{I})\,(\mathbf{v}_i\otimes\mathbf{v}_i) \\ &\quad= (\mathbf{I}\otimes\mathbf{A})(\mathbf{v}_i\otimes\mathbf{v}_i) + (\mathbf{A}\otimes\mathbf{I})(\mathbf{v}_i\otimes\mathbf{v}_i) \\ &\quad= (\mathbf{I}\mathbf{v}_i)\otimes(\mathbf{A}\mathbf{v}_i) + (\mathbf{A}\mathbf{v}_i)\otimes(\mathbf{I}\mathbf{v}_i) \\ &\quad= \mathbf{v}_i\otimes(\lambda_i\mathbf{v}_i) + (\lambda_i\mathbf{v}_i)\otimes\mathbf{v}_i = 2\lambda_i\mathbf{v}_i\otimes\mathbf{v}_i \end{aligned}$$

as required. □

Because in a linear system the asymptotic stability implies that the equilibrium point is hyperbolic, theorem 1 implies $\mathrm{Re}\{\lambda_i\} < 0$ for all $i = 1, \ldots, 2n+2$. Then the linear system (22) is also stable, and $\boldsymbol{\sigma}$ is bounded for all $t \geq 0$. The equilibrium point of (22) is found solving the vectorized Lyapunov equation:

$$(\mathbf{I}\otimes\mathbf{A} + \mathbf{A}\otimes\mathbf{I})\boldsymbol{\sigma} + \mathbf{w} = 0 \tag{23}$$

and because the matrix $(\mathbf{I}\otimes\mathbf{A} + \mathbf{A}\otimes\mathbf{I})$ is regular, the solution is unique. The Lyapunov equation can be solved using Gaussian elimination, with computational complexity $t_1(n) = \mathcal{O}(n^6)$, or with the Bartels-Stewart

algorithm with computational complexity roughly estimated as $t_2(n) = \mathcal{O}(n^3)$ (see the appendix below).

3.2 Nonlinear system analysis

We consider now the case where the elastic potentials include higher order terms. Without loss of generality, we continue to assume that $\bar{\mathbf{x}} = 0$ is the asymptotically stable equilibrium point, and we express the SDE system (10) in the form:

$$d\mathbf{X}_t = (\mathbf{A}\,\mathbf{X}_t + \mathbf{n}(\mathbf{X}_t))\,dt + \mathbf{B}\,dW_t \tag{24}$$

where $\mathbf{X}_t$ and $\mathbf{B}$ are the same state vector and diffusion vector described above, while $\mathbf{A} \in \mathbb{R}^{(2n+2)\times(2n+2)}$ and $\mathbf{n} : \mathbb{R}^{2n+2} \mapsto \mathbb{R}^{2n+2}$ are the linear and nonlinear components of the drift, respectively.[1] In most situations, elastic forces are smooth and odd symmetric, at least for not too large values of the displacement, therefore we can consider $\mathbf{n}(\mathbf{x}) = \mathcal{O}(||\mathbf{x}||^3) \in \mathcal{C}^\infty$. For nonlinear systems the asymptotic stability of $\bar{\mathbf{x}} = 0$ does not imply that the equilibrium point is hyperbolic. Therefore, we shall assume that the origin is also hyperbolic as an explicit additional condition, thus implying that matrix $\mathbf{A}$ is regular.

Because of the nonlinearity, in general we do not expect that the stationary distribution remains a multivariate Gaussian process. Yet, for small enough displacement, it is reasonable that the distribution will remain close enough.

Theorem 3 *Consider system (24), and assume that* $\mathbf{A}$ *is stable, and that* $\mathbf{n}(\mathbf{x})$ *has odd symmetry, i.e.* $\mathbf{n}(-\mathbf{x}) = -\mathbf{n}(\mathbf{x})$. *Then a centered, multivariate normal distribution solves the equation for the first moments.*

Proof Taking expectation in (24), and using the martingale property of Itô integral we obtain the equation for the first moment:

$$\frac{d}{dt}\mathrm{E}[\mathbf{X}_t] = \mathbf{A}\mathrm{E}[\mathbf{X}_t] + \mathrm{E}[\mathbf{n}(\mathbf{X}_t)] \tag{25}$$

Because of the odd symmetry, the Taylor series centered at the origin for $\mathbf{n}(\mathbf{x})$ includes only linear combinations of odd symmetric polynomials of the type $\prod_{j=1}^{N} x_j^{r_j}$, with $\sum_{j=1}^{N} r_j = 2k+1$, $k \in \mathbb{N}$. For a multivariate normal distribution centered at zero, odd order moments, starting with order three, are null, and the first moment equation reduces to

$$\frac{d}{dt}\mathrm{E}[\mathbf{X}_t] = \mathbf{A}\mathrm{E}[\mathbf{X}_t]$$

that has the asymptotic solution $\mathrm{E}[\mathbf{X}_t] = 0$ as required, because $\mathbf{A}$ is stable. □

The equation for the second order moments is obtained again using (24) and Itô formula, as

$$\begin{aligned} d(\mathbf{X}_t\mathbf{X}_t^T) = \big(&\mathbf{A}\mathbf{X}_t\mathbf{X}_t^T + \mathbf{X}_t\mathbf{X}_t^T\mathbf{A}^T + \mathbf{X}_t\mathbf{n}^T(\mathbf{X}_t) \\ &+ \mathbf{n}(\mathbf{X}_t)\mathbf{X}_t^T + \mathbf{B}\mathbf{B}^T\big)dt + \big(\mathbf{B}\mathbf{X}_t^T + \mathbf{X}_t\mathbf{B}^T\big)dW_t \end{aligned} \tag{26}$$

Taking expectations and using the martingale property of Itô integral yields

$$\begin{aligned} \frac{d\boldsymbol{\Sigma}}{dt} = &\mathbf{A}\boldsymbol{\Sigma} + \boldsymbol{\Sigma}\mathbf{A}^T + \mathrm{E}\left[\mathbf{X}_t\mathbf{n}^T(\mathbf{X}_t)\right] \\ &+ \mathrm{E}\left[\mathbf{n}(\mathbf{X}_t)\mathbf{X}_t^T\right] + \mathbf{B}\mathbf{B}^T \end{aligned} \tag{27}$$

Under the assumption that $\mathbf{n}(\mathbf{x}) = \mathcal{O}(||\mathbf{x}||^3)$, it follows that $\mathbf{n}(\mathbf{x})\mathbf{x}^T = \mathcal{O}(||\mathbf{x}||^4)$, and $\mathbf{x}\,\mathbf{n}^T(\mathbf{x}) = \mathcal{O}(||\mathbf{x}||^4)$. Thus, in the differential equation for the second moments, moments of order four appear. In general, the equation for moments of order m can be derived using Itô formula and taking expectations, but this equation would always include the moments of order $m+2$, leading to an open system, formed by an infinite number of linear ODEs.

The system can be closed using a moment closure technique [61]. Moment closure techniques are based on the idea that all moments beyond a certain order can either be neglected, or at least they can be written as functions of lower order moments such as

$$\mathbf{m}_{k+j} = \mathbf{g}_j(\mathbf{m}_1, \ldots, \mathbf{m}_k) \tag{28}$$

where $\mathbf{m}_k$ denotes the k-th order moment, and $\mathbf{g}_j$ is a given function. Different choices for functions $\mathbf{g}_j$ are possible, based for example on some *a priori* assumption on the statistical distribution of the stochastic process. In particular, we observe that for small values of the displacement, we expect that the distribution remains close to a multivariate normal. Moreover,

[1] For the sake of simplicity, we still use the same symbol $\mathbf{A}$ to denote the linear part of the drift.

since $\mathbf{n}(\mathbf{x})$ is odd symmetric, then the components of $\mathbf{x}\,\mathbf{n}^T(\mathbf{x}))$ and of $\mathbf{n}(\mathbf{x})\mathbf{x}^T$ are even symmetric. Thus, we assume that $\mathbf{X}_t \sim \mathcal{N}(0, \boldsymbol{\Sigma}^*)$, and using the properties of the normal distribution we express the fourth order moments as functions of second order moments. Taking vectorization, (27) can be rewritten as

$$\frac{d\boldsymbol{\sigma}}{dt} = (\mathbf{I}\otimes\mathbf{A} + \mathbf{A}\otimes\mathbf{I})\boldsymbol{\sigma} + \mathbf{w} + \varepsilon\mathbf{h}(\boldsymbol{\sigma}) \tag{29}$$

where, as before, $\boldsymbol{\sigma} = \mathrm{vec}(\boldsymbol{\Sigma}) = \mathrm{vec}(\mathrm{E}[\mathbf{X}_t\mathbf{X}_t^T])$, $\varepsilon > 0$ is a parameter that measures the strength of the nonlinearity, and

$$\varepsilon\mathbf{h}(\boldsymbol{\sigma}) = \mathrm{vec}(\mathrm{E}[\mathbf{n}(\mathbf{X}_t)\mathbf{X}_t^T] + \mathrm{E}[\mathbf{X}_t\mathbf{n}^T(\mathbf{X}_t)]). \tag{30}$$

Theorem 4 *For the nonlinear system (29) there exists a neighborhood $\mathcal{B}_\varepsilon(\varepsilon = 0)$ and a branch of equilibrium points $\boldsymbol{\sigma}^*(\varepsilon) \in \mathcal{B}_\varepsilon$, such that*

$$\boldsymbol{\sigma}^*(\varepsilon) = -(\mathbf{I}\otimes\mathbf{A} + \mathbf{A}\otimes\mathbf{I})^{-1} \Big(\mathbf{w} + \varepsilon\mathbf{h}\big(-(\mathbf{I}\otimes\mathbf{A} + \mathbf{A}\otimes\mathbf{I})^{-1}\mathbf{w}\big)\Big) \tag{31}$$

Proof The proof is based on the application of the Implicit Function Theorem. Let $\mathbf{M} = (\mathbf{I}\otimes\mathbf{A} + \mathbf{A}\otimes\mathbf{I})$ and let

$$\mathbf{f}(\varepsilon, \boldsymbol{\sigma}) = \mathbf{M}\boldsymbol{\sigma} + \mathbf{w} + \varepsilon\mathbf{h}(\boldsymbol{\sigma})$$

By theorem 2, and under the hypothesis that $\overline{\mathbf{x}}$ is hyperbolic, matrix $\mathbf{M}$ is regular. Let $\boldsymbol{\sigma}_0 = -\mathbf{M}^{-1}\mathbf{w}$, then $\mathbf{f}(0, \boldsymbol{\sigma}_0) = 0$, and the Jacobian matrix $\frac{\partial\mathbf{f}}{\partial\boldsymbol{\sigma}}\big|_{(0,\boldsymbol{\sigma}_0)} = \mathbf{M}$, is also regular. The implicit function theorem guarantees the existence of a neighborhood $\mathcal{B}_\varepsilon(\varepsilon = 0)$ and of a function $\boldsymbol{\sigma}^*(\varepsilon) : \mathcal{B}_\varepsilon(\varepsilon = 0) \mapsto \mathbb{R}^{(2n+2)(2n+2)}$ such that $\boldsymbol{\sigma}_0 = \boldsymbol{\sigma}^*(0)$ and $\mathbf{f}(\varepsilon, \boldsymbol{\sigma}^*(\varepsilon)) = 0$, for all $\varepsilon \in \mathcal{B}_\varepsilon(\varepsilon = 0)$. For $\varepsilon \ll 1$, we have $\varepsilon\mathbf{h}(\boldsymbol{\sigma}) \approx \varepsilon\mathbf{h}(\boldsymbol{\sigma}_0)$, and (29) can be approximated by

$$\frac{d\boldsymbol{\sigma}}{dt} = \mathbf{M}\boldsymbol{\sigma} + \mathbf{w} + \varepsilon\mathbf{h}(\boldsymbol{\sigma}_0)$$

that admits the equilibrium point

$$\boldsymbol{\sigma}^*(\varepsilon) = -\mathbf{M}^{-1}\left(\mathbf{w} + \varepsilon\mathbf{h}(\boldsymbol{\sigma}_0)\right)$$

as required. □

Using the appropriate components of $\boldsymbol{\sigma}^*(\varepsilon)$, we can calculate the approximate average harvested power and the power efficiency through (14).

3.3 White Gaussian noise limit

Starting from (6), it is easily seen that in the singular limit $\tau \to 0$, Z_t becomes a white Gaussian noise. The results presented in the previous section can be extended to this limiting case. For $\tau \to 0$, the SDE system (10) becomes

$$dQ_j = \frac{1}{m_j}P_j\,dt \tag{32a}$$

$$dP_j = \left[-\frac{\partial U_j(Q_j, Q_{j+1})}{\partial Q_j} - \frac{\partial U_{j-1}(Q_{j-1}, Q_j)}{\partial Q_j} - \frac{\gamma}{m_j}P_j\delta_{1j} - \alpha V\delta_{nj}\right]dt + \delta_{1j}D\,dW_t \qquad j = 1, \ldots, n \tag{32b}$$

$$dV = \left(\frac{\alpha}{C_{\mathrm{pz}}\,m_n}P_n - \frac{G}{C_{\mathrm{pz}}}V\right)dt \tag{32c}$$

The energy stored in the harvester is still given by (11). Using Itô formula and (32) (see appendix) yields

$$dE = \left(-\gamma\frac{P_1^2}{m_1^2} - GV^2 + \frac{D^2}{2m_1}\right)dt + D\frac{P_1}{m_1}dW_t \tag{33}$$

Taking expectations, we obtain the power balance equation

$$\mathrm{E}\left[\frac{dE}{dt}\right] = \frac{D^2}{2m_1} - \frac{\gamma}{m_1^2}\mathrm{E}[P_1^2] - G\mathrm{E}[V^2] \tag{34}$$

The last two terms on the right hand side of (34) are the same as in (13). Conversely, the power injected by the white Gaussian noise is now constant $P_{\mathrm{in}} = D^2/(2m_1)$, so that the conversion efficiency for the energy harvester subject to white Gaussian noise becomes:

$$\eta = \frac{2m_1\,G}{D^2}\mathrm{E}[V^2]. \tag{35}$$

Corollary 1 *If the potentials $U_j(q_j, q_{j+1})$ have a local minimum at $(\overline{q}_j, \overline{q}_{j+1})$ for all $j = 1, \ldots, n$, then*

for $D = 0$ system (32) has an asymptotically stable equilibrium point at $\mathbf{x} = \bar{\mathbf{x}}$.

Proof The proof is completely analogous to that of theorem 1, provided that $\beta = 0$ is substituted in the Lyapunov function $\mathcal{V}(\mathbf{x})$. Note that in this case the Lyapunov function corresponds to the energy stored in the system. □

Concerning the other results derived in the previous section, even them remain valid in the white Gaussian noise limit, where however $\mathbf{x}, \mathbf{B} \in \mathbb{R}^{2n+1}$ are given by:

$$\mathbf{x} = [q_1, p_1, \ldots, q_n, p_n, v]^T, \quad \mathbf{B} = [0, D, 0, \ldots, 0]^T$$

while matrices $\mathbf{A}, \boldsymbol{\Sigma} \in \mathbb{R}^{(2n+1)\times(2n+1)}$ are modified simply removing the last row and the last column from the previous case.

4 Energy harvester optimization

In this section we discuss the optimization of the energy harvester. We shall present a procedure for finding the parameter values, e.g. the masses and the stiffness of the springs, that maximize a given output variable, like the harvested power or the conversion power efficiency. The problem is made challenging by the absence of closed form formulas for calculating the output variables. A naive approach would consist of numerically integrating the SDE system (10) (or the equivalent system (32), in the case of white Gaussian noise), and then evaluate the averages. Obviously, this approach becomes unfeasible when a large parameter space must be explored.

Recently, optimization methods have received renewed attention because of their relevance in machine learning applications [62]. Optimization algorithms can be roughly classified as first-order, higher-order, and derivative-free methods. First-order methods, like the gradient descent/ascent, rely on the knowledge of the gradient of the objective function to help direct the search for an extremum. High-order methods converge faster but require more information and may face challenges related to the operation and storage of the inverse of the Hessian matrix. Finally, derivative-free methods are ideally well suited for problems where the derivative of the objective function does not exist or is difficult to calculate, instead, they rely on heuristic or empirical search rules [62].

In this work, we exploit the gradient ascent method, complemented by Nesterov's momentum, for the optimization of the nonlinear energy harvester. However, as an analytical formula for the objective function (typically the maximum output power, or the maximum power efficiency) is not available, we shall compute the derivatives numerically, using the approximate solution provided by (31).

The goal is to maximize one of the components of the covariance matrix $\boldsymbol{\Sigma}$ (or the vectorized version $\boldsymbol{\sigma}$). We denote the objective function by $\sigma^* : P \subseteq \mathbb{R}^p \mapsto \mathbb{R}$, representing a nonlinear mapping between the p-dimensional parameter space P, and the set of real numbers, and we denote with $\boldsymbol{\mu} \in P \subseteq \mathbb{R}^p$ the vector of parameters.

The problem is formulated as follows: find

$$\boldsymbol{\mu}^* = \arg\max_{\boldsymbol{\mu}\in P} \sigma^*(\boldsymbol{\mu}) \tag{36}$$

We start with an initial guess for the optimum parameter set $\boldsymbol{\mu} = \boldsymbol{\mu}_1$, and the momentum $\mathbf{v} = \mathbf{v}_1 = 0$, and we solve the stationary Lyapunov equation (23) with:

$$\mathbf{A} = \mathbf{A}_{(\boldsymbol{\mu}_k + \nu\mathbf{v}_k)} = \mathbf{A}(\boldsymbol{\mu}_k + \nu\mathbf{v}_k)$$

and

$$\mathbf{W} = \mathbf{W}_{(\boldsymbol{\mu}_k + \nu\mathbf{v}_k)} = \mathrm{vec}\big(\mathbf{B}(\boldsymbol{\mu}_k + \nu\mathbf{v}_k)\mathbf{B}^T(\boldsymbol{\mu}_k + \nu\mathbf{v}_k)\big)$$

where the hyper-parameter ν is the momentum decay. The solution of the Lyapunov equation $\boldsymbol{\sigma}_k$ is used to evaluate the nonlinear function $\mathbf{h}(\boldsymbol{\sigma}_k, \boldsymbol{\mu}_k + \nu\mathbf{v}_k)$, and the nonlinear equation (31) is solved finding $\boldsymbol{\sigma}_k^*$.

To calculate the direction of steepest variation, the derivatives are calculated as follows. First the i-th component of the vector $(\boldsymbol{\mu}_k + \nu\mathbf{v}_k)$ is changed by a small amount

$$(\boldsymbol{\mu}_k + \nu\mathbf{v}_k)_i \to (\boldsymbol{\mu}_k + \nu\mathbf{v}_k)_i + \delta$$

Then, Eqs. (23) and (31) are solved again for this new value, finding $\widetilde{\sigma}_{k,i}$, and $\widetilde{\sigma}^*_{k,i}$, and the derivative is approximated by the difference quotient:

$$\frac{\partial\sigma^*}{\partial\boldsymbol{\mu}_{k,i}} \approx \frac{\widetilde{\sigma}^*_{k,i} - \sigma^*_{k,i}}{\delta} \tag{37}$$

The procedure is repeated for each component of $\boldsymbol{\mu}_k$, and the velocity and the parameter vector are updated according to:

$$\mathbf{v}_{k+1} = \nu \mathbf{v}_k + \theta \, \nabla \sigma^* \tag{38a}$$

$$\boldsymbol{\mu}_{k+1} = \boldsymbol{\mu}_k + \mathbf{v}_{k+1} \tag{38b}$$

where the hyper-parameter $\theta > 0$ is the leaning rate.

The procedure is repeated until each component of the variation vector $\boldsymbol{\Delta} = |\boldsymbol{\mu}_{k+1} - \boldsymbol{\mu}_k|$ is less than a fixed threshold, indicating that the objective function is close to a stationary point, or until a maximum number of iteration is reached.

Algorithm 1: Gradient ascent algorithm with Nesterov's momentum for the optimization of a non-linear energy harvester.

Input : $\boldsymbol{\mu_1}$, $\mathbf{v}_1$, initial guess for parameters values and momentum.
Output: $\boldsymbol{\mu^*} = \arg\max \sigma^*(\boldsymbol{\mu})$.

Set the values for the hyper-parameters: θ, gradient ascent step; ν momentum decay; $\Delta_{\min}$, increment tolerance
Set parameters: δ, increment for differentiation; $k_{\max}$, maximum number of iterations
Set $k = 1$ and $\boldsymbol{\Delta}$ such that: $\min \boldsymbol{\Delta}(i) > \Delta_{\min}$
while $\min \boldsymbol{\Delta}(i) > \Delta_{min}$ && $k < k_{max}$ **do**
    Value of the output function. Solve: $\mathbf{A}_{(\boldsymbol{\mu}_k+\nu\mathbf{v}_k)}\boldsymbol{\Sigma} + \boldsymbol{\Sigma}\mathbf{A}^T_{(\boldsymbol{\mu}_k+\nu\mathbf{v}_k)} + \mathbf{W}_{(\boldsymbol{\mu}_k+\nu\mathbf{v}_k)} = 0$ for $\boldsymbol{\sigma}_k = \mathrm{vec}(\boldsymbol{\Sigma})$
    Solve: $\boldsymbol{\sigma}^*_k = -\mathbf{M}^{-1}_{(\boldsymbol{\mu}_k+\nu\mathbf{v}_k)}(\mathrm{vec}(\mathbf{W}_{(\boldsymbol{\mu}_k+\nu\mathbf{v}_k)}) + \varepsilon\mathbf{h}(\boldsymbol{\sigma}_k))$
    for *each element of* $\boldsymbol{\mu}_k + \nu\mathbf{v}_k$ **do**
        Solve: $\mathbf{A}_{(\boldsymbol{\mu}_k+\nu\mathbf{v}_k)_i+\delta}\boldsymbol{\Sigma} + \boldsymbol{\Sigma}\mathbf{A}^T_{(\boldsymbol{\mu}_k+\nu\mathbf{v}_k)_i+\delta} + \mathbf{W}_{(\boldsymbol{\mu}_k+\nu\mathbf{v}_k)_i+\delta} = 0$ for $\widetilde{\boldsymbol{\sigma}}_k = \mathrm{vec}(\boldsymbol{\Sigma})$
        Solve: $\widetilde{\boldsymbol{\sigma}}^*{}_k = -\mathbf{M}^{-1}_{(\boldsymbol{\mu}_k+\nu\mathbf{v}_k)_i+\delta}\big(\mathrm{vec}(\mathbf{W}_{(\boldsymbol{\mu}_k+\nu\mathbf{v}_k)_i+\delta}) + \varepsilon\mathbf{h}(\widetilde{\boldsymbol{\sigma}}_k)\big)$
        Calculate: $\dfrac{\partial\sigma^*}{\partial\boldsymbol{\mu}_{k,i}} = \dfrac{\widetilde{\sigma}^*_{k,i} - \sigma^*_{k,i}}{\delta}$
    end
    Update: $\mathbf{v}_{k+1} = \nu\mathbf{v}_k + \theta\,\nabla\sigma^*$
    $\boldsymbol{\mu}_{k+1} = \boldsymbol{\mu}_k + \mathbf{v}_{k+1}$
    $k = k + 1$
    $\boldsymbol{\Delta} = |\boldsymbol{\mu}_{k+1} - \boldsymbol{\mu}_k|$
end
Solve $\mathbf{A}_{\boldsymbol{\mu}^*}\boldsymbol{\Sigma} + \boldsymbol{\Sigma}\mathbf{A}^T_{\boldsymbol{\mu}^*} + \mathbf{W}_{\boldsymbol{\mu}^*} = 0$ for $\boldsymbol{\sigma}_{\boldsymbol{\mu}^*} = \mathrm{vec}(\boldsymbol{\Sigma})$
Solve $\boldsymbol{\sigma}^*{}_{\boldsymbol{\mu}^*} = -\mathbf{M}^{-1}_{\boldsymbol{\mu}^*}\big(\mathrm{vec}(\mathbf{W}_{\boldsymbol{\mu}^*}) + \varepsilon\mathbf{h}(\boldsymbol{\sigma}_{\boldsymbol{\mu}^*})\big)$

The gradient descent/ascent algorithm is very efficient if the objective function is smooth enough. Local minima, in the form of "narrow valleys" aligned with the gradient direction are not a particular problem. Conversely, if the gradient crosses over the valley, many steps must be taken in order to make progress along the valley's floor [63]. Another issue is the presence of saddle points. Approaching a saddle, the gradient becomes rather close to zero, and the method may select too small step sizes and thus take a long time to cross the nearly flat surface. Adding small amount of stochasticity to the gradient, also called stochastic gradient descent/ascent, may be beneficial to overcome the problem, as well as to escape from local minima [63].

An alternative solution to improve convergence rate is to use an adaptive learning rate that automatically adjusts to the changing landscape, for example in the form of a momentum that accumulates at each step [64,65]. The Nesterov's momentum method included in algorithm 1 is one of such methods. For $\nu = 0$, we recover gradient descent. For $\nu \neq 0$, momentum accumulates at each step of the gradient ascent, and the learning rate adapts consequently. The gradient is evaluated after adding momentum, which brings the next step closer to the minimum/maximum.

5 Numerical results

In this section we report on the numerical analysis of the networked energy harvesting systems, described by the SDE systems (10) and (32), and we compare these results with the theoretical predictions. We consider both single and multiple mass-spring energy harvesters, composed by n masses connected through springs with elastic potentials of the form:

$$U(q_j, q_{j+1}) = \frac{1}{2}k_j(q_j - q_{j+1})^2 + \frac{1}{4}\bar{k}_j(q_j - q_{j+1})^4 \tag{39}$$

where k_j and $\bar{k}_j$ are the stiffness constants (in N/m and N/m^3, respectively), and as usual $q_{n+1} = 0$. The SDE systems have been integrated numerically using a stochastic Runge-Kutta, strong order 1, numerical integration scheme. The numerical simulations were run using time integration step $dt = 1\ \mu$s, and time length $\Delta T = 100$ s. In each simulations we used random initial conditions, and we have removed the initial 3 s, roughly corresponding to the length of the transient, resulting in $97 \cdot 10^6$ samples for each simulation. The

Table 1 Values of the fixed parameters used in the simulations

Parameter	Value
γ	0.12 kg/s
D	10^{-1} N
α	0.0042 N/V (Am/s)
m_n, m	10 g
k_n, k	1 kN/m
$\overline{k}_n, \overline{k}$	1 kN/m^3
C_{pz}	80.08 nF
R	1 MΩ

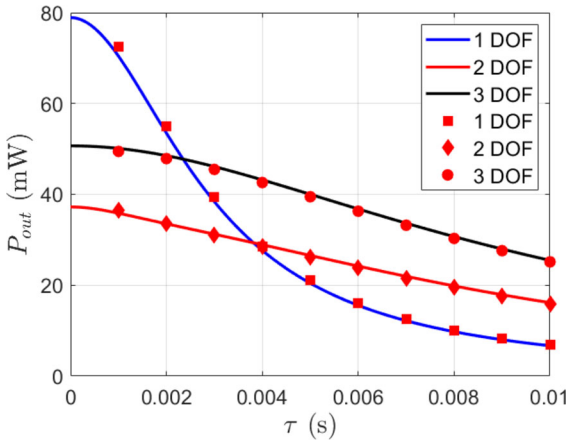

Fig. 2 Average output power for a single mechanical DOF and multi mechanical DOF networked energy harvesters, as a function of the noise correlation time τ. Parameters are summarized in Tables 1 and 2. Solid lines are theoretical predictions obtained through the approximated method. Markers are averages from numerical simulations

reported results have been obtained through averaging over ten or more simulations.

For our analysis we have considered the masses m_i $(i = 1, ..., n-1)$ and the stiffness coefficients k_i, $\overline{k}_i$, $(i = 1, ..., n-1)$ as free parameters to be optimized. All other parameters, including the mass m_n and the stiffness coefficients k_n, $\overline{k}_n$ (denoted simply m, k and $\overline{k}$ for the single DOF harvester) are kept fixed. For simplicity, we used $\overline{k}_i = k_i$ in magnitude, for all $i = 1, \ldots, n$. The values of the fixed parameters are summarized in Table 1.

Figure 2, shows the average output power, as a function of the noise correlation time τ for a energy harvester with one, two, and three mass-spring pairs, respectively. Solid lines are the theoretical predictions, obtained using the method described in Sect. 3, while markers are numerical results, obtained averaging over 10 simulations. The very good agreement between theoretical and numerical simulations can be understood as a consequence of the relatively small displacements, effectively limiting the contributions of the nonlinear terms. Masses and springs stiffness have been optimized for noise correlation time $\tau = 0.01$ s, where the energy harvesters with two and three mass-spring pairs clearly outperform the single mass-spring harvester. The power performances, and the values of the free parameters used in the simulations, are summarized in Table 2.

Irrespective of the number of mass-spring pairs, the scavenged power of the harvesters decreases as the noise correlation time τ increases, with maximum harvested power at $\tau = 0$ s, corresponding to the white Gaussian noise. This result is not surprising considering that, according to (9), the PSD of the OU process has a cutoff frequency at $\omega_0 = 1/\tau$ and therefore, the power available for scavenging is a monotonic decreasing function of τ. White Gaussian noise, with its flat PSD, contains in principle an infinite amount of power. Although this behavior is obviously not realistic from the point of view of physics, white noise is still a valid approximation when the cutoff frequency is very high compared with the harvester resonance frequency. For the single mass-spring harvester, in particular, the scavenged power shows a pronounced decrease with the correlation time. In contrast, harvesters with multiple mass-spring pairs are more robust, therefore being advisable whenever the noise correlation time is expected to be high. From Table 2, we can see that increasing the number of mechanical DOF in the networked energy harvester offers diminishing returns. In particular, increasing the number of DOF from three to four offers a minimum gain in the harvested power, whereas the increase in computational cost for the optimization is significant. Therefore, there is no significant advantage in considering very large numbers of DOF.

Our analysis shows that adding more mass-spring pairs can improve the scavenged energy according to two mechanisms. The first mechanism consists in increasing the efficiency. Figure 3 shows that for the single mass-spring harvester, the power injected by the noise is systematically higher than that for the mass-spring pairs system (with the two curves converging for $\tau > 0.01$ s). Yet, being more efficient, the latter offers higher average output power for all $\tau > 0.004$

Table 2 Power performances and values of the free parameters used in the simulations. Values are calculated using $\tau = 0.01$ s, and $\bar{k}_j = k_j$ in magnitude

DOF	P_{out}	P_{in}	η	Parameters
1	6.85 mW	39.02 mW	0.18	$m = 10$ g
				$k = 1$ kN/m
2	15.86 mW	33.75 mW	0.47	$m_1 = 65.1$ g
				$m_2 = 10.0$ g
				$k_1 = 2$ kN/m
				$k_2 = 1$ kN/m
3	25.14 mW	137.22 mW	0.18	$m_1 = 17.1$ g
				$m_2 = 65.1$ g
				$m_3 = 10.0$ g
				$k_1 = 0.2$ kN/m
				$k_2 = 2$ kN/m
				$k_3 = 1$ kN/m
4	26.00 mW	135.00 mW	0.19	$m_1 = 18.9$ g
				$m_2 = 32.2$ g
				$m_3 = 50.0$ g
				$m_4 = 10.0$ g
				$k_1 = 0.2$ kN/m
				$k_2 = 2$ kN/m
				$k_3 = 2$ kN/m
				$k_3 = 1$ kN/m

s. The second mechanism is to increase the energy "absorbing capacity" of the harvester. Again, Fig. 3 shows that the harvester with three mass-spring pairs absorbs more power than the two stage system for all τ, and absorbs more power than the single stage harvester for all $\tau > 2.64$ ms. Because the efficiency of the harvester with three mass-springs pair is about the same as the single pair one, the higher output power of the former can be completely ascribed to its higher capacity to absorb energy from random vibrations.

We investigate the role of the nonlinearities in Fig. 4. The figure shows the average output power calculated with the method described in Sect. 3, compared with the average power calculated through numerical simulations, as functions of the nonlinear stiffness coefficient. The average output powers are normalized to the average power of the linearized system. Blue squares are the average power calculated with the method of Sect. 3, while black diamonds are numerical results, obtained averaging over 30 simulations. Vertical bars are the error (one standard deviation) from numerical

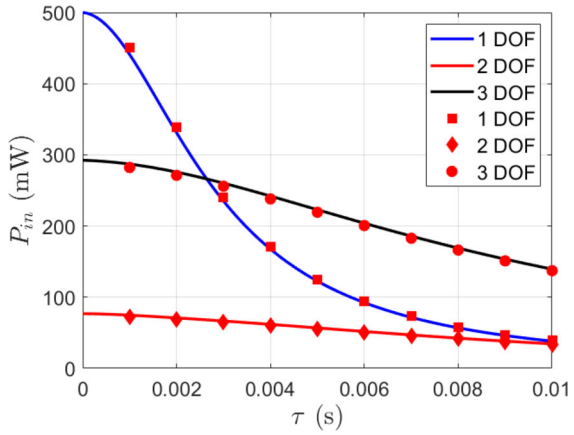

Fig. 3 Average input power for a single mechanical DOF and multi mechanical DOF networked energy harvesters, as a function of the noise correlation time τ. Parameters are summarized in Tables 1 and 2. Solid lines are theoretical predictions obtained through the approximated method. Markers are averages from numerical simulations

simulations. The top part of the figure refers to the system with one mechanical DOF, while the lower part is relative to the system with two mechanical DOF. For both systems the noise intensity was set to the relatively high value $D = 5$ N, which leads to unrealistic high harvested powers, to emphasize the effect of the nonlinear terms. The figures shows that the approximate analytical method offers reliable results for a wide range of values of $\bar{k}$, even for the limiting case of high noise intensity.

Finally, Fig. 5 shows the average output power as a function of the mass m_1, and of the spring compliance $1/k_1$ (that is used instead of the stiffness k_1 for the sake of the figure's clarity), for a two mass-spring pairs harvester. For reference, the average output power was calculated with a grid search, using a 100×100 grid of equally spaced points with $0 < m_{1,i} \leq 0.1$ kg, and $0 < 1/k_{1,i} \leq 0.01$ m/N. Red and yellow markers illustrate the application of the gradient ascent optimization algorithm, for two different choices of the initial parameters' values $\boldsymbol{\mu}_1 = [m_1, k_1]^T$. The average output power is a rather smooth function, and as a consequence the gradient ascent algorithm is very efficient in finding the maximum and converges very fast. As it is well known, convergence of gradient based algorithms is strongly influenced by the learning rate θ and the tolerance $\Delta_{\min}$. There are no established criteria to chose the hyper-parameters, rather one has to rely on intuition and experience. In this case, our simu-

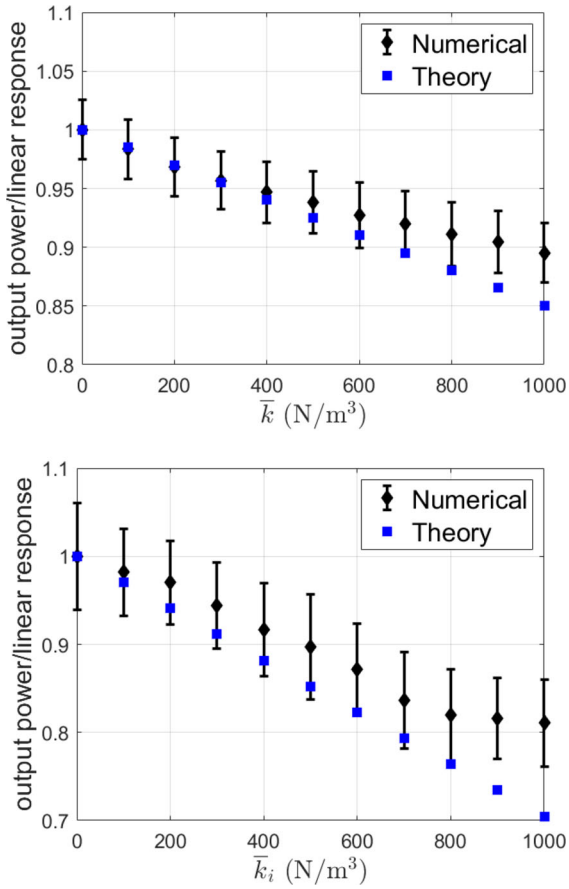

Fig. 4 Average output power normalized to the power of the linearized system, as a function of the nonlinear stiffness coefficients. Upper part: one mechanical DOF energy harvester. Lower part: two mechanical DOF energy harvester, with $\overline{k}_1 = \overline{k}_2$. Noise intensity is $D = 5$ N. Other parameters values are summarized in Table 1

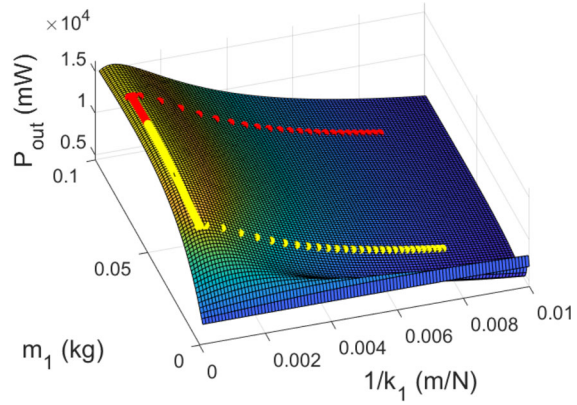

Fig. 5 Average output power versus the mass m_1 and the compliance $1/k_1$ for a two DOF energy harvesters. Noise correlation time is $\tau = 0.01$ s. Other parameters' value are those of Table 1. Red and yellow markers are trajectories of the gradient ascent optimization algorithm

lations shows that the addition of momentum increases the converge rate by about a 3%.

6 Conclusions

We have presented the analysis, design and optimization of networked energy harvesters for ambient mechanical vibrations. The proposed architecture can be schematically represented as a set of inertial masses, connected pairwise through nonlinear elastic springs, forming a chain of coupled nonlinear resonators. The networked harvester is equivalent to a mechanical filter, where the masses and the elastic constant of the springs can be optimized to maximize the scavenged energy or the power efficiency.

The mechanical filter collects kinetic energy from ambient vibrations, and convert it into electrical power through a piezoelectric transducer. Ambient vibrations are modeled as an Ornstein–Uhlenbeck, process, i.e as a low-pass filtered white Gaussian noise. This is a reasonable model for ambient vibrations in complex environment, whenever most of the energy is concentrated at low frequencies.

The equations of motion for the harvester have been derived, and semi-analytical formulas for the average harvested power and the power efficiency have been obtained using stochastic calculus. The theoretical predictions have been confirmed through numerical Monte-Carlo simulations, showing an excellent degree of accuracy.

An optimization algorithm based on the gradient ascent method, combined with Nesterov's momentum, has been presented. The average harvested power has been used as a goal function. Because the goal function is semi-analytical, a numerical procedure has been developed to evaluate the derivatives and the gradient. The goal function is a smooth function of the parameters, the gradient ascent method is very efficient, and it shows excellent convergence. Application of Nesterov's momentum guarantee a certain speed up of the convergence, helping the algorithm to move over crests of the goal function's landscape.

Our analysis shows that the addition of few mechanical degrees-of-freedom offers significant advantages both in terms of average harvested power and power efficiency, without the drawbacks of previously proposed solutions based on purely electrical impedance matching. Finally, we discuss how the networked energy harvester improves the scavenged power by either increasing the harvesting efficiencies, or increasing the amount of power absorbed from mechanical vibrations.

Acknowledgements This research has been conducted with the support of the Italian inter-university PhD course in Sustainable Development and Climate Change.

Author contributions All authors contributed equally to the paper

Funding Open access funding provided by Politecnico di Torino within the CRUI-CARE Agreement. The authors have not disclosed any funding.

Data availability The data that support the findings of this study are available from the corresponding author upon reasonable request.

Declarations

Conflict of interest The authors declare no conflict of interest.

Open Access This article is licensed under a Creative Commons Attribution 4.0 International License, which permits use, sharing, adaptation, distribution and reproduction in any medium or format, as long as you give appropriate credit to the original author(s) and the source, provide a link to the Creative Commons licence, and indicate if changes were made. The images or other third party material in this article are included in the article's Creative Commons licence, unless indicated otherwise in a credit line to the material. If material is not included in the article's Creative Commons licence and your intended use is not permitted by statutory regulation or exceeds the permitted use, you will need to obtain permission directly from the copyright holder. To view a copy of this licence, visit http://creativecommons.org/licenses/by/4.0/.

Appendix: Itô formula and the energy equations

Let $\mathbf{X}_t = [X_{1t}, X_{2t}, \ldots, X_{nt}]^T$ be a vector of Itô processes, solution of the Itô SDE

$$d\mathbf{X}_t = \mathbf{a}(\mathbf{X}_t)dt + \mathbf{B}(\mathbf{X}_t)d\mathbf{W}_t \tag{40}$$

and let $g : [0, +\infty[\times \mathbb{R}^n \mapsto \mathbb{R}$, $g(t, \mathbf{x}) \in \mathcal{C}^2$. Then $g(t, \mathbf{x})$ is also an Itô process, and it satisfies [57,59]

$$dg = \frac{\partial g(t,\mathbf{X})}{\partial t}dt + \sum_{i=1}^{n} \frac{\partial g(t,\mathbf{X})}{\partial x_i} dX_{it} + \frac{1}{2}\sum_{i,j=1}^{n} \frac{\partial^2 g(t,\mathbf{X})}{\partial x_i \partial x_j} dX_{it}\, dX_{jt} \tag{41}$$

where $dt^2 = dt\, dW_i = 0$, and $dW_i\, dW_j = \delta_{ij} dt$. Equation (41) is called Itô formula.

From equation (10), we have:

$$dQ_i\, dQ_j = dQ_i\, dP_j = dP_i\, dP_j = dQ_i\, dV = = dP_i\, dV = dV^2 = 0 \tag{42}$$

Using Itô formula, the SDE for the energy is:

$$dE = \sum_{i=1}^{n} \left[\frac{\partial E}{\partial q_i} dQ_i + \frac{\partial E}{\partial p_i} dP_i \right] + \frac{\partial E}{\partial V} dV \tag{43}$$

Combining together equations (10) and (11), the energy equation (12) easily follows.

For the white Gaussian noise, using equation (32) we have $(dP_1)^2 = D^2\, dt$, while all other equality in (42) remain valid. Thus the energy equation becomes

$$dE = \sum_{i=1}^{n} \left[\frac{\partial E}{\partial q_i} dQ_i + \frac{\partial E}{\partial p_i} dP_i \right] + \frac{\partial E}{\partial V} dV + \frac{1}{2} \frac{\partial^2 E}{\partial p_1^2} dP_1^2 \tag{44}$$

that after substitution gives equation (33).

Appendix: Lyapunov equation

Given two matrices $\mathbf{A}$, $\mathbf{W} \in \mathbb{R}^{n,n}$, the matrix equation

$$\mathbf{A}\,\mathbf{X} + \mathbf{X}\mathbf{A}^T = \mathbf{W} \tag{45}$$

is called Lyapunov equation.

Different algorithms exists for solving the Lyapunov equation depending on the properties of $\mathbf{A}$ and $\mathbf{W}$. A naive approach is to take vectorization, thereby obtaining the solution:

$$\mathbf{X} = (\mathbf{I} \otimes \mathbf{A} + \mathbf{A} \otimes \mathbf{I})^{-1} \mathrm{vec}(\mathbf{W}) \tag{46}$$

provided that matrix $\mathbf{A}$ is regular (see theorem 2).

The linear system of n^2 equations in (45) can be solved using Gaussian elimination with computational complexity $t(n) = \mathcal{O}(n^6)$. This approach may be convenient for small n, due to its simplicity, but it becomes unfeasible for large n.

The Bartels-Stewart algorithm [66–68] is the standard method for the efficient solution of the Lyapunov equation. All real matrices have Shur decomposition

$$\mathbf{A} = \mathbf{Q}\mathbf{T}\mathbf{Q}^T \tag{47}$$

where $\mathbf{Q}$ is an orthogonal matrix, and $\mathbf{T}$ is a block triangular matrix

$$\mathbf{T} = \begin{bmatrix} \mathbf{T}_{11} & \dots & \mathbf{T}_{1r} \\ & \ddots & \vdots \\ & & \mathbf{T}_{rr} \end{bmatrix} \tag{48}$$

with $\mathbf{T}_{jj} \in \mathbb{R}^{n_j,n_j}$, being $n_j \in \{1, 2\}$, $j = 1, \dots, r$ and $\sum_{j=1}^{r} n_j = n$. Multiplying (45) to the left by $\mathbf{Q}^T$ and to the right by $\mathbf{Q}$, we obtain

$$\mathbf{Q}^T\mathbf{W}\mathbf{Q} = \mathbf{T}\mathbf{Y} + \mathbf{Y}\mathbf{T}^T \tag{49}$$

Where $\mathbf{Y} = \mathbf{Q}^T\mathbf{X}\mathbf{Q}$. Next, we introduce matrices

$$\mathbf{Q}^T\mathbf{W}\mathbf{Q} = \begin{bmatrix} \mathbf{C}_{11} & \mathbf{C}_{12} \\ \mathbf{C}_{21} & \mathbf{C}_{22} \end{bmatrix}, \qquad \mathbf{Y} = \begin{bmatrix} \mathbf{Z}_{11} & \mathbf{Z}_{12} \\ \mathbf{Z}_{21} & \mathbf{Z}_{22} \end{bmatrix}, \qquad \mathbf{T} = \begin{bmatrix} \mathbf{R}_{11} & \mathbf{R}_{12} \\ 0 & \mathbf{R}_{22} \end{bmatrix} \tag{50}$$

where $\mathbf{Z}_{22}$, $\mathbf{C}_{22}$, $\mathbf{T}_{22} = \mathbf{R}_{22} \in \mathbb{R}^{n_r,n_r}$. The triangularized problem can be solved by separating the blocks, obtaining:

$$\mathbf{C}_{11} = \mathbf{R}_{11}\mathbf{Z}_{11} + \mathbf{R}_{12}\mathbf{Z}_{21} + \mathbf{Z}_{11}\mathbf{R}_{11}^T + \mathbf{Z}_{12}\mathbf{R}_{12}^T \tag{51a}$$
$$\mathbf{C}_{12} = \mathbf{R}_{11}\mathbf{Z}_{12} + \mathbf{R}_{12}\mathbf{Z}_{22} + \mathbf{Z}_{12}\mathbf{R}_{22}^T \tag{51b}$$
$$\mathbf{C}_{21} = \mathbf{R}_{22}\mathbf{Z}_{21} + \mathbf{Z}_{21}\mathbf{R}_{11}^T + \mathbf{Z}_{22}\mathbf{R}_{12}^T \tag{51c}$$
$$\mathbf{C}_{22} = \mathbf{R}_{22}\mathbf{Z}_{22} + \mathbf{Z}_{22}\mathbf{R}_{22}^T \tag{51d}$$

If $n_r = 1$, then

$$Z_{22} = \frac{C_{22}}{2R_{22}} \tag{52}$$

Otherwise, if $n_r = 2$

$$\mathrm{vec}(\mathbf{Z}_{22}) = (\mathbf{I} \otimes \mathbf{R}_{22} + \mathbf{R}_{22} \otimes \mathbf{I})^{-1}\mathrm{vec}(\mathbf{C}_{22}) \tag{53}$$

Introducing $\mathbf{Z}_{22}$ in (51b) and in the transpose of (51c), we obtain

$$\widetilde{\mathbf{C}}_{12} = \mathbf{C}_{12} - \mathbf{R}_{12}\mathbf{Z}_{22} = \mathbf{R}_{11}\mathbf{Z}_{12} + \mathbf{Z}_{12}\mathbf{R}_{22}^T \tag{54a}$$
$$\widetilde{\mathbf{C}}_{21} = \mathbf{C}_{21}^T - \mathbf{R}_{12}\mathbf{Z}_{22}^T = \mathbf{R}_{11}\mathbf{Z}_{21}^T + \mathbf{Z}_{21}^T\mathbf{R}_{22}^T \tag{54b}$$

System (54) takes the form

$$\mathbf{D} = \mathbf{U}\mathbf{X} + \mathbf{X}\mathbf{R}_{22}^T \tag{55}$$

where $\mathbf{U}$ is upper triangular. Similarly to (52)-(53), $\mathbf{X}_j$ can be computed from a smaller linear system

$$\mathrm{vec}(\mathbf{X}_j) = (\mathbf{I} \otimes \mathbf{T}_{jj} + \mathbf{R}_{22} \otimes \mathbf{I})^{-1}\mathrm{vec}(\widetilde{\mathbf{W}}_j) \tag{56}$$

Algorithm 2: Bartels-Stewart algorithm for the Lyapunov equation.

Input : $\mathbf{A}$, $\mathbf{W} \in \mathbb{R}^{n,n}$, $\mathbf{W} = \mathbf{W}^T$.
Output: $\mathbf{X} = \mathbf{X}^T$, solving (45).

Compute Schur decomposition $\mathbf{T} = \mathbf{Q}^T\mathbf{A}\mathbf{Q}$, with $\mathbf{Q}\mathbf{Q}^T = \mathbf{Q}^T\mathbf{Q} = \mathbf{I}$, and establish $n_1, \dots, n_r$, $\mathbf{T}_{11}, \dots, \mathbf{T}_{rr}$ according to (48).
Set $\mathbf{C} = \mathbf{Q}^T\mathbf{W}\mathbf{Q}$, and $m = n$.
while $k > 1$ **do**
  Set $m = m - n_k$.
  Partition $\mathbf{C}$ into $\mathbf{C}_{11}, \mathbf{C}_{12}, \mathbf{C}_{21}, \mathbf{C}_{22}$ according to (50), with $\mathbf{C}_{22} \in \mathbb{R}^{n_k,n_k}$.
  Set $\mathbf{R}_{22} = \mathbf{T}_{kk}$ and

$$\mathbf{R}_{11} = \begin{bmatrix} \mathbf{T}_{11} & \dots & \mathbf{T}_{1,k-1} \\ & \ddots & \vdots \\ & & \mathbf{T}_{k-1,k-1} \end{bmatrix}, \quad \mathbf{R}_{12} = \begin{bmatrix} \mathbf{T}_{1k} \\ \vdots \\ \mathbf{T}_{k-1,k} \end{bmatrix}$$

  Find $\mathbf{Z}_{22}$ using (52) or (53).
  Compute $\widetilde{\mathbf{C}}_{12}, \widetilde{\mathbf{C}}_{21}$ using (54).
  Solve for $\mathbf{Z}_{12} \in \mathbb{R}^{m,n_k}$ and $\mathbf{Z}_{21} \in \mathbb{R}^{n_k,m}$ using (56) with $p = k$.
  Store $\mathbf{Y}(1 : m, m + (1 : n_k)) = \mathbf{Z}_{12}$
  Store $\mathbf{Y}(m + (1 : n_k), 1 : m) = \mathbf{Z}_{21}$
  Store $\mathbf{Y}(m + (1 : n_k), m + (1 : n_k)) = \mathbf{Z}_{22}$
  Set $\mathbf{C} := \mathbf{C}_{11} - \mathbf{R}_{12}\mathbf{Z}_{21} - \mathbf{Z}_{12}\mathbf{R}_{12}^T$
  k = k-1
end
Return solution: $\mathbf{X} = \mathbf{Q}\mathbf{Y}\mathbf{Q}^T$

Solving (56) for $j = p-1, \ldots, 1$ for both of (54) we find $\mathbf{Z}_{12}$ and $\mathbf{Z}_{21}$. Introducing $\mathbf{Z}_{12}$, $\mathbf{Z}_{21}$ and $\mathbf{Z}_{22}$ in (51a) gives a new Lyapunov equation of size $n-p$, and the procedure is then iterated for the reduced system.

Considering that both the Shur decomposition and the while cycle require roughly n^3 operations, the complexity of the Bartels-Stewart algorithm is if order

$$t(n) = \mathcal{O}(n^3)$$

References

1. Paradiso, J.A., Starner, T.: Energy scavenging for mobile and wireless electronics. IEEE Pervasive Comput. **4**(1), 18–27 (2005)
2. Beeby, S.P., Tudor, M.J., White, N.M.: Energy harvesting vibration sources for microsystems applications. Meas. Sci. Technol. **17**(12), R175 (2006)
3. Priya, S., Inman, D.J.: Energy Harvesting Technologies. Springer, Berlin (2009)
4. Roundy, S., Wright, P.K., Rabaey, J.M.: Energy Scavenging for Wireless Sensor Networks. Springer, New York (2003)
5. Yang, G.-Z. (ed.): Body Sensor Networks, vol. 1. Springer, London (2006)
6. Penella-López, M.T., Gasulla-Forner, M.: Powering Autonomous Sensors An Integral Approach with Focus on Solar and RF Energy Harvesting. Springer London, Limited (2011)
7. Chong, Y.-W., Ismail, W., Ko, K., Lee, C.-Y.: Energy harvesting for wearable devices: A review. IEEE Sens. J. **19**(20), 9047–9062 (2019)
8. Mitcheson, P.D., Green, T.C., Yeatman, E.M., Holmes, A.S.: Architectures for vibration-driven micropower generators. J. Microelectromech. Syst. **13**(3), 429–440 (2004)
9. Roundy, S.: On the effectiveness of vibration-based energy harvesting. J. Intell. Mater. Syst. Struct. **16**(10), 809–823 (2005)
10. Renno, J.M., Daqaq, M.F., Inman, D.J.: On the optimal energy harvesting from a vibration source. J. Sound Vib. **320**(1–2), 386–405 (2009)
11. Gammaitoni, L., Neri, I., Vocca, H.: The benefits of noise and nonlinearity: extracting energy from random vibrations. Chem. Phys. **375**(2), 435–438 (2010)
12. Kwon, S.-D., Park, J., Law, K.: Electromagnetic energy harvester with repulsively stacked multilayer magnets for low frequency vibrations. Smart Mater. Struct. **22**(5), 055007 (2013)
13. Almoneef, T.S., Erkmen, F., Ramahi, O.M.: Harvesting the energy of multi-polarized electromagnetic waves. Sci. Rep. **7**(1), 1–14 (2017)
14. Erkmen, F., Almoneef, T.S., Ramahi, O.M.: Electromagnetic energy harvesting using full-wave rectification. IEEE Trans. Microw. Theory Tech. **65**(5), 1843–1851 (2017)
15. Ujihara, M., Carman, G.P., Lee, D.-G.: Thermal energy harvesting device using ferromagnetic materials. Appl. Phys. Lett. **91**(9), 093508 (2007)
16. Cuadras, A., Gasulla, M., Ferrari, V.: Thermal energy harvesting through pyroelectricity. Sens. Actuators, A **158**(1), 132–139 (2010)
17. Tan, Y.K., Panda, S.K.: Energy harvesting from hybrid indoor ambient light and thermal energy sources for enhanced performance of wireless sensor nodes. IEEE Trans. Ind. Electron. **58**(9), 4424–4435 (2010)
18. Lefeuvre, E., Badel, A., Richard, C., Petit, L., Guyomar, D.: A comparison between several vibration-powered piezoelectric generators for standalone systems. Sens. Actuators, A **126**(2), 405–416 (2006)
19. Choi, W.J., Yongbae Jeon, J.-H., Jeong, R.S., Kim, S.-G.: Energy harvesting mems device based on thin film piezoelectric cantilevers. J. Electroceram. **17**(2–4), 543–548 (2006)
20. Cook-Chennault, K.A., Thambi, N., Sastry, A.M.: Powering mems portable devices. a review of non-regenerative and regenerative power supply systems with special emphasis on piezoelectric energy harvesting systems. Smart Mater. Struct. **17**(4), 043001 (2008)
21. Erturk, A., Inman, D.J.: Piezoelectric Energy Harvesting. John Wiley & Sons, Hoboken (2011)
22. Priya, S., Song, H.-C., Zhou, Y., Varghese, R., Chopra, A., Kim, S.-G., Kanno, I., Liao, W., Ha, D.S., Ryu, J., Polcawich, R.G.: A review on piezoelectric energy harvesting: materials, methods, and circuits. Energy Harvest. Syst. **4**(1), 3–39 (2017)
23. Covaci, C., Gontean, A.: Piezoelectric energy harvesting solutions: a review. Sensors **20**(12), 3512 (2020)
24. Beeby, S.P., Torah, R.N., Tudor, M.J., Glynne-Jones, P., O'donnell, T., Saha, C.R., Roy, S.: A micro electromagnetic generator for vibration energy harvesting. J. Micromech. Microeng. **17**(7), 1257 (2007)
25. Mann, B.P., Sims, N.D.: Energy harvesting from the nonlinear oscillations of magnetic levitation. J. Sound Vib. **319**(1–2), 515–530 (2009)
26. Elvin, N.G., Elvin, A.A.: An experimentally validated electromagnetic energy harvester. J. Sound Vib. **330**(10), 2314–2324 (2011)
27. Cottone, F., Basset, P., Vocca, H., Gammaitoni, L., Bourouina, T.: Bistable electromagnetic generator based on buckled beams for vibration energy harvesting. J. Intell. Mater. Syst. Struct. **25**(12), 1484–1495 (2014)
28. Kucab, K., Górski, G., Mizia, J.: Energy harvesting in the nonlinear electromagnetic system. Eur. Phys. J. Spec. Top. **224**(14–15), 2909–2918 (2015)
29. Caruso, G., Galeani, S., Menini, L.: Semi-active damping and energy harvesting using an electromagnetic transducer. J. Vib. Control **24**(12), 2542–2561 (2018)
30. Costanzo, L., Schiavo, A.L., Sarracino, A., Vitelli, M.: Stochastic thermodynamics of an electromagnetic energy harvester. Entropy **24**(9), 1222 (2022)
31. Wang, L., Yuan, F.G.: Vibration energy harvesting by magnetostrictive material. Smart Mater. Struct. **17**(4), 045009 (2008)
32. Narita, F., Fox, M.: A review on piezoelectric, magnetostrictive, and magnetoelectric materials and device technologies for energy harvesting applications. Adv. Eng. Mater. **20**(5), 1700743 (2018)

33. Clemente, C.S., Davino, D., Loschiavo, V.P.: Analysis of a magnetostrictive harvester with a fully coupled nonlinear fem modeling. IEEE Trans. Magn. **57**(6), 1–4 (2021)
34. Clemente, C.S., Davino, D., Iannone, I., Loschiavo, V.P.: Experimental characterization of an ac-dc boost for energy harvesting device based on magnetostrictive materials. Electricity **5**(1), 24–35 (2024)
35. Stanton, S.C., McGehee, C.C., Mann, B.P.: Reversible hysteresis for broadband magnetopiezoelastic energy harvesting. Appl. Phys. Lett. **95**(17), 174103 (2009)
36. Tang, L., Yang, Y., Soh, C.K.: Toward broadband vibration-based energy harvesting. J. Intell. Mater. Syst. Struct. **21**(18), 1867–1897 (2010)
37. Yan, Z., Sun, W., Hajj, M.R., Zhang, W., Tan, T.: Ultra-broadband piezoelectric energy harvesting via bistable multi-hardening and multi-softening. Nonlinear Dyn. **100**, 1057–1077 (2020)
38. Zhemin Wang, Y.D., Li, T., Yan, Z., Tan, T.: A flute-inspired broadband piezoelectric vibration energy harvesting device with mechanical intelligent design. Appl. Energy **303**, 117577 (2021)
39. Malaji, P.V., Friswell, M.I., Adhikari, S., Litak, G.: High-energy orbit harvesting with torsionally coupled mistuned pendulums. J. Vib. Eng. Technol. **11**(8), 4223–4240 (2023)
40. De, S.L., Muralidharan, A., Ali, S.F.: Role of inertial nonlinearity and coupling stiffness on a series of coupled harvesters. Appl. Math. Model. **136**, 115631 (2024)
41. Bonnin, M., Traversa, F.L., Bonani, F.: Leveraging circuit theory and nonlinear dynamics for the efficiency improvement of energy harvesting. Nonlinear Dyn. **104**(1), 367–382 (2021)
42. Bonnin, M., Traversa, F.L., Bonani, F.: An impedance matching solution to increase the harvested power and efficiency of nonlinear piezoelectric energy harvesters. Energies **15**(8), 2764 (2022)
43. Bonnin, M., Song, K.: Frequency domain analysis of a piezoelectric energy harvester with impedance matching network. Energy Harvest. Syst. **10**(1), 119–133 (2022)
44. Song, K., Bonnin, M., Traversa, F.L., Bonani, F.: Stochastic analysis of a bistable piezoelectric energy harvester with a matched electrical load. Nonlinear Dyn. **111**(18), 16991–17005 (2023)
45. Lossouarn, B., Aucejo, M., Deü, J.-F., Multon, B.: Design of inductors with high inductance values for resonant piezoelectric damping. Sens. Actuators A **259**, 68–76 (2017)
46. Kim, I.-H., Jung, H.-J., Lee, B.M., Jang, S.-J.: Broadband energy-harvesting using a two degree-of-freedom vibrating body. Appl. Phys. Lett. **98**(21), 1 (2011)
47. Hao, W., Tang, L., Yang, Y., Soh, C.K.: A novel two-degrees-of-freedom piezoelectric energy harvester. J. Intell. Mater. Syst. Struct. **24**(3), 357–368 (2013)
48. Zhu, W.Q., Cai, G.Q., Hu, R.C.: Stochastic analysis of dynamical system with double-well potential. Int. J. Dyn. Control **1**(1), 12–19 (2013)
49. Hoffmann, D., Folkmer, B., Manoli, Y.: Experimental analysis of a coupled energy harvesting system with monostable and bistable configuration. In: Journal of Physics: Conference Series, vol. 557, p. 012134. IOP Publishing (2014)
50. Fu, Y., Ouyang, H., Benjamin Davis, R.: Nonlinear dynamics and triboelectric energy harvesting from a three-degree-of-freedom vibro-impact oscillator. Nonlinear Dyn. **92**(4), 1985–2004 (2018)
51. Sun, W., Jang, H., Seok, J.: Magnetically coupled piezoelectric galloping-based energy harvester using a tandem configuration. Mech. Syst. Signal Process. **161**, 107952 (2021)
52. Li, X., Meng, J., Yang, C., Zhang, H., Zhang, L., Song, R.: A magnetically coupled electromagnetic energy harvester with low operating frequency for human body kinetic energy. Micromachines **12**(11), 1300 (2021)
53. Sani, G., Bednarek, M., Witkowski, K., Awrejcewicz, J.: Dynamics and energy harvesting from parametrically coupled self-excited electromechanical oscillator. Nonlinear Dyn. **112**, 11785–11802 (2024)
54. Akinaga, H.: Recent advances and future prospects in energy harvesting technologies. Jpn. J. Appl. Phys. **59**(11), 110201 (2020)
55. Bonnin, M., Song, K., Traversa, F.L., Bonani, F.: A circuit theory perspective on the modeling and analysis of vibration energy harvesting systems: A review. Computation **11**(3), 45 (2023)
56. Rosso, M., Cuccurullo, S., Perli, F.P., Maspero, F., Corigliano, A., Ardito, R.: A method to enhance the nonlinear magnetic plucking for vibration energy harvesters. Meccanica **59**(9), 1577–1592 (2024)
57. Gardiner, C.W., et al.: Handbook of Stochastic Methods, vol. 3. Springer, Berlin (1985)
58. Bonnin, M., Traversa, F.L., Bonani, F.: Analysis of influence of nonlinearities and noise correlation time in a single-DOF energy-harvesting system via power balance description. Nonlinear Dyn. **100**(1), 119–133 (2020)
59. Øksendal, B.: Stochastic Differential Equations, 6th edn. Springer-Verlag, Berlin (2003)
60. Bacciotti, A., Rosier, L.: Liapunov Functions and Stability in Control Theory. Springer Science & Business Media, Berlin (2005)
61. Kuehn, C.: Moment closure–a brief review. Control of self-organizing nonlinear systems, pp. 253–271 (2016)
62. Sun, S., Cao, Z., Zhu, H., Zhao, J.: A survey of optimization methods from a machine learning perspective. IEEE Transactions on Cybernetics **50**(8), 3668–3681 (2019)
63. Kochenderfer, M.J., Wheeler, T.A.: Algorithms for Optimization. MIT Press, Cambridge (2019)
64. Bubeck, S., et al.: Convex optimization: Algorithms and complexity. Found. Trends Mach. Learn. **8**(3–4), 231–357 (2015)
65. Lessard, L., Recht, B., Packard, A.: Analysis and design of optimization algorithms via integral quadratic constraints. SIAM J. Optim. **26**(1), 57–95 (2016)
66. Bartels, R.H., Stewart, G.W.: Solution of the matrix equation AX + XB= C [F4]. Commun. ACM **15**(9), 820–826 (1972)
67. Sorensen, D.C., Zhou, Y.: Direct methods for matrix Sylvester and Lyapunov equations. J. Appl. Math. **2003**(6), 277–303 (2003)
68. Simoncini, V.: Computational methods for linear matrix equations. SIAM Rev. **58**(3), 377–441 (2016)

Publisher's Note Springer Nature remains neutral with regard to jurisdictional claims in published maps and institutional affiliations.